

**Seasonal Predictability of Primary East-Asian Summer
Circulation Patterns by Three Operational Climate Prediction
Models**

Fang ZHOU^{1,2}, Hong-Li REN^{2,3}, Zeng-Zhen HU⁴, Ming-Hong LIU², Jie WU², and
Chang-Zheng LIU²

¹*Climate Change Research Center, Institute of Atmospheric Physics, and Nansen–Zhu
International Research Centre, Chinese Academy of Sciences, Beijing 100029, China*

²*Laboratory for Climate Studies & CMA-NJU Joint Laboratory for Climate
Prediction Studies, National Climate Center, China Meteorological Administration,
Beijing 100081, China*

³*Department of Atmospheric Science, School of Environmental Studies, China
University of Geoscience, Wuhan 430074, China*

⁴*Climate Prediction Center, NCEP/NWS/NOAA, 5830 University Research Court,
College Park, MD 20740, USA*

Aug 2019

Revised to QJRMS

This is the author manuscript accepted for publication and has undergone full peer review but has not been through the copyediting, typesetting, pagination and proofreading process, which may lead to differences between this version and the [Version of Record](#). Please cite this article as doi: [10.1002/qj.3697](https://doi.org/10.1002/qj.3697)

- *Corresponding author address:* Hong-Li Ren, National Climate Center, China
Meteorological Administration, 46 Zhongguancun Nandajie St., Haidian District,
Beijing 100081, China. E-mail: renhl@cma.gov.cn

This work was jointly supported by the National Key Research and Development Program on monitoring, Early Warning and Prevention of Major Natural Disaster (Grant No. 2018YFC1506004, 2017YFC1502302), and the Foundation for Innovative Research Groups of the National Natural Science Foundation of China (Grant No. 41421004).

Funding information

This work is supported by National Key Research and Development Program of China (Grant No. 2018YFC1506004, 2017YFC1502302); National Natural Science Foundation of China (Grant No. 41421004).

ABSTRACT

Seasonal predictability of the Primary East-Asian Summer Circulation Patterns (PEASCPs), including the Western Pacific Subtropical High (WPSH), South Asian High (SAH), anomalous Philippine Sea AntiCyclone (PSAC), and East Asian Summer Monsoon (EASM), are investigated by using the hindcasts from the three operational climate prediction models, including BCC_CSM1.1(m), NCEP CFSv2, and ECMWF System 4. We show that prediction skills of the indices for representing these PEASCPs are sensitive to the initial calendar month of model prediction, and the ensemble mean of the three models provides relatively higher and more stable skills than forecasts from individual model. In general, the indices of intensity and area have high prediction skills while the position indices have relatively low skills. Specifically, the skills of the WPSH intensity, area, SAH center intensity, PSAC and EASM are higher, while the skills of the WPSH western boundary and SAH center latitude are lower, and the skills of WPSH ridge line and SAH center longitude are the lowest. Further analysis shows that the El Niño-South Oscillation (ENSO) has a large contribution to these prediction skills and these patterns of atmospheric circulation anomalies in response to ENSO can be well captured by models, which is the major predictability source of the skills.

Key words: Primary East-Asian summer circulation patterns (PEASCPs), prediction

skills, predictability source, El Niño and South Oscillation (ENSO).

Author Manuscript

1. Introduction

China is located in the East Asian monsoon region where the climate is complex and variable. Floods, droughts and other climate extremes caused by large scale circulation anomalies in East Asia and West Pacific Ocean often give rise to great losses of economy and people's life. Climate anomalies in China are directly impacted by some Primary East-Asian Summer Circulation Patterns (PEASCPs), including the Western Pacific Subtropical High (WPSH), South Asian High (SAH), anomalous Philippine Sea AntiCyclone (PSAC) as well as East Asian Summer Monsoon (EASM) (Ding and Chan, 2005; Xue et al., 2015). From the climate perspective, predicting the PEASCP is of a great importance for rainfall and surface air temperature prediction and disaster prevention (Wang et al., 2009; Zhou and Zuo, 2010; Wang et al., 2015).

The WPSH, SAH and PSAC are primary members of EASM system and are associated with the atmospheric circulation variation in East Asia. WPSH is a permanent anticyclonic circulation in Northwest Pacific, its variability is affected by El Niño-South Oscillation (ENSO), plays a vital role in the ENSO-EASM connection (Wang et al., 2000; Wu et al., 2003; Xie et al., 2009; Wu et al., 2009). For example, in El Niño year, positive anomalies of sea surface temperature (SST) in the central equatorial Pacific affect EASM, through generate anomalous anticyclones in the Philippines Sea area (Wang et al., 2000). PSAC is a large-scale anomalous

anticyclonic circulation over the western North Pacific and usually significant when El Niño happens. It can be regarded as the concrete physical manifestation of WPSH change and plays an important role of linking the climatic anomalies over East Asia and tropical Pacific. SAH is located over the Tibetan-Iran Plateau during summer time and it is the most powerful and stable anticyclonic circulation pattern in the global upper troposphere. The variations of its intensity and position have a close relationship with the onset and variability of the EASM system, as well as the meridional migration of the rain belt in eastern China (Zhang et al., 2000, Zhang and Wu, 2001; Qian et al., 2002; Ding and Wang, 2005; Liu et al., 2013; Wei et al., 2015).

The evolutions of PEASCPs are quantitatively represented in the form of indices. For example, dozens of monsoon indices have been defined by using different atmosphere circulation variables, such as zonal and meridional wind at 200 hPa and 850 hPa (Wu and Ni, 1997; Lu and Chan, 1999; Wang and Fan, 1999; Lau, 2000; Wang, 2001, 2002; Zhang et al., 2003), outgoing longwave radiation (Zhou et al., 2003), equivalent potential temperature (Wang and Fan, 1999), land-sea thermal and dynamic contrast (Guo, 1983; Shi et al, 1996; Sun et al., 2002; Zhao and Zhou, 2009). There are also multiple indices to be used to measure the various aspects of WPSH, including the meridional and zonal location indices (Lu, 2002), intensity, area, longitude of western boundary, and latitude of ridge line indices (Liu et al., 2012;

Wang et al., 2013; Yang et al., 2017). For SAH, its intensity, area and position indices are normally defined with reference of specified geopotential height contour at 100 hPa or 200 hPa (Zhang et al., 2000, Qian et al., 2002). Wei et al. (2015) also proposed an east-west shift index and north-south shift index to quantify the position changes of SAH. The definition of PSAC index is relatively simple that the area average of sea level pressure (SLP) anomalies over the Philippine Sea region is the most widely used index (Wang et al., 2000; Wang and Zhang, 2002).

Since the atmospheric general circulation models forced by prescribed lower boundary conditions had shown reasonable skill in seasonal monsoon prediction for the past decades (Zeng et al., 1990, 1997; Shukla, 1998; Kang et al., 2002; Wang et al., 2004; Zhou et al., 2009), they nevertheless exhibit noticeable shortcomings due to the lack of air–sea interaction, which is extremely important for the EASM system (e.g., Wang et al., 2005; Wu and Kirtman, 2005). Coupled ocean-atmosphere dynamical model prediction systems have gradually made great progress and can offer overall better performance, and have become the major tool of dynamical climate prediction in recent decades (Palmer et al., 2004; Kumar et al., 2005; Li et al., 2005; Wang et al., 2005; Kug et al., 2008; National Research Council, 2010; Ma and Wang, 2014). For example, the majority of East Asian climate phenomena such as WPSH, EASM, and some SST modes like ENSO and Indian Ocean basin mode (IOBM) can be accurately

captured nearly half a year in advance at the Beijing Climate Center (Ren et al., 2017). In addition, multi-model ensemble (MME) has become a routine approach in climate prediction (Krishnamurti et al., 1999; Kharin et al., 2002; Palmer and Coauthors, 2004; Min et al., 2009; Weisheimer et al., 2009; Kirtman et al., 2014; Yang et al., 2016). One of advantages of MME is to reduce random errors in forecast caused by defaults of individual models and by uncertainty of initial conditions (ICs) of forecast (Zhu et al., 2013; Han et al., 2016).

Based on the hindcast data from the three operational climate prediction models, including Beijing Climate Center Climate System Model version 1.1 with moderate resolution (BCC_CSM1.1(m)) (Wu et al., 2014), National Center for Environmental Prediction/Climate Forecast System version 2 (NCEP CFSv2) (Saha et al., 2014), and European Centre for Medium-range Weather Forecasts (ECMWF) System 4 (Molteni et al., 2011), this study focuses on examining performance of seasonal prediction of these PEASCPs and relevant attribution of their predictability source. Through this analysis, the model abilities in predicting the PEASCPs will be revealed. The paper is organized as follows. Models, data and method are introduced in section 2. Prediction skills of the PEASCPs are examined in section 3. Predictability source is investigated in section 4, and a summary with discussions is finally given in section 5.

2. Models, data and method

2.1 Models and observational data

The hindcasts for seasonal prediction used in this study are generated by three coupled ocean–atmosphere dynamical models, including BCC_CSM1.1(m), NCEP CFSv2, and ECMWF System 4. Information about prediction time, initialized date, and time period of each model data is illustrated in Table 1. Details for these three models can be found in <http://forecast.bccsm.ncc-cma.net/web/channel-63.htm>, <http://cfs.ncep.noaa.gov>, and <https://www.ecmwf.int/en/elibrary/11209-new-ecmwf-seasonal-forecast-system-system-4>, respectively. These three operational climate prediction models are used to conduct MME. In this study, for convenience of calculation, when the intensity and area indices are calculated, the horizontal resolution of data will be unified to $2.5^{\circ} \times 2.5^{\circ}$ latitude/longitude, while for the position index calculation, the data are interpolated onto a $0.1^{\circ} \times 0.1^{\circ}$ latitude/longitude grid by using bilinear interpolation.

Here, we only examine the prediction skill in boreal summer. There are total of 26 boreal summers (1991–2016) which are available for all the three models. For prediction evaluations, observational PEASCP indices are calculated by using the NECP–Department of Energy (NCEP-DOE) reanalysis (R2) data (Kanamitsu et al., 2002). The summer is referred to the average of June-July-August (JJA).

2.2 Indices and prediction skill evaluation method

In this work, the prediction capacities of PEASCPs are evaluated based on a set of reconstructed indices which can objectively characterize the activities of PEASCPs and are convenient for calculation and suitable for climate prediction operation. Taken WPSH as an example, we should not only pay attention to the variation of its intensity and range, but also to the change of its position, which has an important influence on the location of rain belt and the extend of monsoon. Therefore the intensity, area, western boundary, and ridge line indices proposed by (Liu et al., 2012) are utilized to describe the WPSH. Also, to depict the changes in SAH strength and location, center intensity, latitude, and longitude indices will be applied (Zhang et al., 2000, Qian et al., 2002). The PSAC index is defined as the area average of SLP anomalies over the Philippine Sea region according to Wang et al. (2000). Two EASM indices are used in this study: One is defined by Zhang et al. (2003) as the difference of 850 hPa zonal wind anomalies between tropical monsoon trough area in East Asia and subtropical East Asia (denoted as EASM-Z03), the other (denoted as EASM-H04) is defined based on the East Asia-Pacific (EAP) teleconnection pattern (Huang, 2004). Details of each index are shown in Table 2. In addition, PEASCPs possess a long-term trend due to climate variation. In climate prediction operation, we believe that trends should be part of the prediction that needs to be accurately estimated. Therefore, in this study,

the prediction skills are calculated without removing linear trends.

The Temporal Correlation Coefficient (TCC) is used to measure the prediction skill. The calculation formula is given as:

$$TCC_i = \frac{\sum_{j=1}^N (p_{i,j} - \bar{p}_i)(x_j - \bar{x})}{\sqrt{\sum_{j=1}^N (p_{i,j} - \bar{p}_i)^2} \sqrt{\sum_{j=1}^N (x_j - \bar{x})^2}}$$

where i denotes the initial month and j denotes the target year JJA. $p_{i,j}$ represents the predicted year j JJA mean index initialized on month i , \bar{p}_i represents the average of predicted JJA mean indices initialized on month i of each year. x_j expresses the observational index in year j and \bar{x} expresses the average of x_j . $N=26$ from 1991 to 2016.

Unlike TCC, the Pattern Correlation Coefficient (PCC) reflects the similarity of anomalous spatial patterns between the prediction and observation. The calculation formula is as follows:

$$PCC_j = \frac{\sum_{i=1}^M \Delta x_{i,j} \Delta p_{i,j}}{\sqrt{\sum_{i=1}^M \Delta x_{i,j}^2} \sqrt{\sum_{i=1}^M \Delta p_{i,j}^2}}$$

where j denotes the target year JJA and i denotes the grid point. $\Delta p_{i,j}$ and $\Delta x_{i,j}$ represent the predicted and observational year j JJA mean value anomaly on grid i respectively. M is the total number of the grid points over the evaluated spatial region.

3. Prediction Skills of the PEASCPs

3.1 Prediction of the WPSH

To evaluate the prediction ability of WPSH, the model-predicted JJA mean WPSH indices are calculated using the model hindcast data. Then, TCCs between observed and predicted WPSH indices are calculated to represent the prediction skills. Considering that the NCEP CFSv2 seasonal forecast consists of 9-month predictions while the ECMWF System 4 only has 7-month predictions, JJA mean forecast only can be initiated from previous November by the NCEP CFSv2 and from February by the ECMWF System 4, respectively.

Figure 1 shows the prediction skills for JJA mean WPSH intensity, area, western boundary, and ridge line indices as a function of initial calendar months. Overall, the BCC_CSM1.1(m), NCEP CFSv2, and ECMWF System 4 models all have high capabilities to predict the intensity, area and western boundary of WPSH. The TCC scores of intensity, area and western boundary indices exceed 0.6 and pass the significance test at 99% confidence level for the forecast initiated in November. TCC scores gradually increase with the initial month approaching JJA. However, the ridge line index is poorly predicted with most of TCC scores less than 0.2 in most initial months. Only for ECMWF System 4 model and the ensemble mean in June, their TCC scores exceed 0.4. It is suggested that the meridional position variation of WPSH is relatively difficult to predict accurately.

Comparing the prediction performances of WPSH indices by the three models, we can find that the capacity of BCC_CSM1.1(m) model is slightly better than the other two models, while the NCEP CFSv2 model is the weakest. However, the ensemble mean does not show a prominent advantage for increasing the skill but can provide more stable skills than forecasts from individual models.

3.2 Prediction of the SAH

The prediction skill of SAH is evaluated via examining the TCCs of SAH center intensity, center latitude, and center longitude indices as shown in Figure 2. Compared with the WPSH, the prediction skill of SAH is lower, especially for the position indices. For the intensity index, TCC score exceeds 0.6 for all forecasts initiated in November-June. Though TCC score in June is slightly higher than other months, prediction skill does not increase obviously with the initial month approaching JJA. The performance of BCC_CSM1.1(m) model is a little bit better than NCEP CFSv2 and ECMWF System 4 models, and the ensemble mean can stabilize the TCC score nearly 0.7 for forecasts with IC since February.

The capacity of SAH center latitude prediction is worse than the center intensity. The performance of ECMWF System 4 model is better than the other two, and the ensemble mean can stabilize the TCC score above 0.4 since February. It is worth noting that the maximum prediction skill of SAH center latitude by BCC_CSM1.1(m)

model is about 0.8 at the lead time of 0 month, initiated in June, but sharply decays to 0.4 at the lead time of 1 month. Such a similar phenomenon can also be seen in the WPSH prediction that TCC scores of BCC_CSM1.1(m) model at lead 0 month is higher than NCEP CFSv2 and ECMWF System 4. It is probably related to the different time/day of ICs within a month used by each model.

Models have a much lower capability to predict the SAH center longitude position. The model prediction skill is only significant for forecast with IC in June by BCC_CSM1.1(m) model and in April by ECMWF System 4 model, while there are almost no prediction skills for other initial months. Predictions initialized before March, the TCC scores are even negative.

3.3 Prediction of the PSAC

The prediction skill of summer PSAC is shown in Figure 3. The TCC score decreases slowly as the lead time increasing. It is interesting to see that the TCC score of ECMWF System 4 model can reach 0.8 with ICs in May and June, and BCC_CSM1.1(m) model can exceed the 95% confidence level as the initial time up to November. That means that the models can provide a useful prediction for PSAC as initialized from prior autumn.

3.4 Prediction of the EASM

Figure 4 gives the TCC scores of the two EASM indices. Overall, the

EASM-Z03 index has higher prediction skills than the EASM-H04 index. In particular, the TCC score of EASM-Z03 index reaches about 0.7 at the initial month of June and declines slowly that remains higher than 0.5 at initial time of February. As a comparison, the EASM-H04 index shows lower skill with some fluctuations. For predictions initialized in December and January, the TCC scores of BCC_CSM1.1(m) model can exceed the 95% significance level. With ICs in February and June, NCEP CFSv2 model can provide useful predictions. Capacity of ECMWF System 4 model is relatively weak, but ensemble mean of these three models produces stable prediction skills initiating from February. It is worth mentioning that the calculation of EASM-H04 index only requires three grid points, which may cause some uncertainty. If a model simulation has some deviations in spatial pattern, it will bring biases in index grid selection. Thus, it may be a reason why the prediction skills of EASM-H04 index show some fluctuations, especially in BCC_CSM1.1(m) model. In general, these results indicate that models are able to provide skillful predictions of the EASM, but the skill of prediction is dependent on the definitions of the EASM indices (Liu et al., 2015; Cheng et al. 2016).

It can be summarized from the above analyses that intensity and area indices of these PEASCPs have higher prediction skills than the position indices. Except for the WPSH western boundary, most of the prediction skills of position indices are low.

4. Attributions of Predictability Sources

In section 3 we have evaluated the prediction skill of PEASCPs, and found that most of the WPSH, SAH, PSAC, and EASM indices have high predictability in the models. To explore the sources of prediction skills in models, take the WPSH as an example, we put the observed and predicted time series of the WPSH intensity, area, and western boundary indices together to show the dispersion in different years, as shown in Figure 5.

It can be seen that during the strong WPSH years, such as 1998, 2010 and 2016, the predicted intensity and area indices are highly consistent with the observations, especially in BCC_CSM1.1(m) and ECMWF System 4 models. The prediction bias of NCEP CFSv2 model is relatively large, but the ensemble mean can largely remove the forecast biases and improve the prediction. Although the prediction skill of western boundary index is lower than intensity and area indices, we can still find that the predictions are more consistent with observations during strong WPSH years than normal years, especially in ECMWF System 4 model.

Not only the WPSH indices, the SAH center intensity, PSAC, and EASM-Z03 indices are also well predicted in 1998, 2010 and 2016 summer, as shown in Figure 6. The predicted indices are highly similar with the observations no matter when the initial month is. Prediction biases of NCEP CFSv2 model seem relatively larger than

BCC_CSM1.1(m) and ECMWF System 4 models. Noting that the strong El Niño events occurred during 1997/98, 2009/10, and 2015/16 winters, we can infer that the WPSH, SAH, PSAC, EASM appear to be well predicted during years with strong ENSO forcing, suggesting the possible impact of ENSO on East Asian summer climate variability (Wu et al, 2003).

Furthermore, to examine the impact of strong ENSO events on the prediction skill, we exclude the years of 1998, 2010 and 2016, and recalculate the TCC scores of WPSH intensity, area, western boundary, SAH center intensity, PSAC and EASM-Z03 indices, as shown in Figure 7. Compared with Figures 1 to 4, it can be seen that the TCC scores are obviously decreased in the forecasts without the three El Niño years. The averaged reductions of WPSH intensity and area indices are larger than 0.2 in each model, while the reduction of WPSH western boundary index is even more than 0.3. The skills of some other indices, such as the SAH center intensity and PSAC, also decrease visibly to different extents. These overall declines of the forecast skills by excluding the extreme large anomaly years imply that predictabilities are higher in years with large anomaly than with small anomaly, consisting with signal-noise consideration (Kumar and Hoerling 2000, Hu et al. 2019).

To further examine the contribution of ENSO to prediction skills, we calculated the lead-lag correlation coefficients between the observed JJA-mean WPSH, SAH,

PSAC and EASM indices and monthly Niño3.4 index. The Niño3.4 index is obtained from National Oceanic and Atmospheric Administration/Climate Prediction Center (NOAA/CPC, <https://www.cpc.ncep.noaa.gov/data/indices/>). We can see that the indices having high prediction skills such as the WPSH intensity, area, SAH center intensity, PSAC and EASM-Z03 indices have large lag-correlations with Niño3.4 index, which pass the significance at 99% confidence level (Figure 8). The highest correlation coefficients occur during former October to January, implying that the PEASCPs may be affected by ENSO. Nevertheless, some indices having low prediction skills, such as the WPSH ridge line, SAH center latitude, SAH center longitude and EASM-H04 indices, are poorly correlated with the Niño3.4 index. The WPSH western boundary index appears to be negatively correlated with the winter Niño3.4 index but does not pass the significance at 95% confidence level. Therefore, when strong ENSO events occur in observation during former winter, and if the models capture the high lag-correlation ship between PEASCPs and ENSO, the prediction of PEASCPs is largely reliable.

Based on such assumption, we calculate the lead-lag correlation coefficients between the model-predicted JJA-mean WPSH, SAH, PSAC and EASM indices and the observed monthly Niño3.4 index, as shown in Figures 9 and 11. Taking the WPSH intensity index as an example, we can see that the model-predicted indices have high

lag-correlations with the observed Niño3.4 index. No matter which month the prediction initiated, the correlation coefficients always achieve above 0.7 in former winter and pass the significance at 99% confidence level. This lag-correlation pattern is captured by all the three models, but still have some differences. In the BCC_CSM1.1(m) and NCEP CFSv2 models, correlation coefficients assume quite dissimilar by different initial months and that may correspond to the distinct prediction skills from former November to June. But in the ECMWF System 4 model, correlation coefficients represent almost the same and result in stable prediction skills initialized from February to June. As expected, the lag-correlation coefficients of ensemble mean show virtually identical for different initial months. Result is similar for other indices with high prediction skills such as the WPSH area, WPSH western boundary.

To further understand the contributions of ENSO to the high prediction skill for WPSH, we also show the spatial pattern of the skills of H500 for ensemble mean for initial months in Feb to Jun, and then compare it with lag correlation of DJF Niño 3.4 index on predicted JJA H500, as shown in Figure 10. It is clear that in the Western Pacific, regions with high prediction skills also have significant high correlation ship with ENSO. Other regions such as the North Pacific, North India Ocean, and some parts of Eurasia, prediction skills of H500 is lower, and the correlation between these

areas and ENSO is similarly not very high. This may be evidence that ENSO is a major source of high prediction skills of circulation patterns (like WPSH) in the Northwest Pacific region.

The results of SAH, PSAC, and EASM indices are shown in Figure 11. Although the correlation between the SAH center latitude index and the Niño3.4 index is not high, the BCC_CSM1.1(m) and ECMWF System 4 models still well capture the lag correlation pattern. But the NCEP CFSv2 model doesn't reproduce this correlation pattern and that may be why the prediction skills are lower than other models.

In observations, the EASM-H04 index is poorly correlated with the Niño3.4 index, but this correlation is overstated by BCC_CSM1.1(m) and ECMWF System 4 models, which may lead to the prediction skills of BCC_CSM1.1(m) and ECMWF System 4 models lower than NCEP CFSv2 in most initial months. Other poorly predicted indices such as the WPSH ridge line and SAH center longitude indices don't have the significant correlation with ENSO in observation. Therefore, the correlations in models do not have much reference.

ENSO events are the most important predictability source of seasonal prediction in East Asia (Wu et al., 2003; Wang et al., 2009). Since the TCC skills of BCC_CSM1.1(m), NCEP CFSv2 and ECMWF System 4 models for Niño3.4 index are all larger than 0.7 at 6 months lead (Ren et al., 2017, Saha et al., 2014, Molteni et

al., 2011), the capacities of models to predict PEASCP indices may rely onto the relationship between the prediction performance of circulation field and ENSO. Scatter plots of PCC skills for models initiated in May against the absolute value of former winter-(December, January and February, DJF)-mean Niño3.4 index is shown in Figure 12. We can see that there is some positive correlation between the prediction skills of models and the amplitude of Niño3.4 index, particularly seen in geopotential height at 200 hPa over South Asia and 500 hPa over Western Pacific (Significant correlation coefficients at 90% and 95% confidence levels are about 0.32 and 0.38, respectively). When the amplitude of Niño3.4 index is larger, the PCC scores of models are generally higher. Although the correlation of zonal wind at 200 hPa over South Asia is relatively small, but ensemble mean still reaches 90% confidence level. Besides, zonal wind at 850 hPa over Southeast Asia also shows positive correlation. Accordingly, at the time of the ENSO events (whether El Niño or La Niña), the prediction skills of models will be remarkably improved. It is possible to draw a conclusion that ENSO is the most important predictability source of models to predict circulation patterns in East Asia. The enhancement of circulation pattern prediction skills mainly stems from the high prediction skills of ENSO.

However, although there are some linear relationships between ENSO intensity and prediction skills (Figure 12), the spread is extremely large. That may imply that

other processes, such as land surface, stratosphere, internal dynamical processes (National Research Council, 2010), and some other tropical air-sea interactions may play important role in summer climate variability in East Asia, which are relatively independent to ENSO. For example, Watanabe and Jin (2002) demonstrated that the Indian Ocean warming and the Tibetan Plateau essentially contribute to the development of PSAC. More recently, a mechanism based on seasonally-dependent, moist, static-energy advection has been proposed in an effort to interpret the onset of the PSAC and its eastward movement from South Asia (Chou, 2004). Therefore, the spread shown in Figure 12 may be a consequence of the common primary feature of climate variability over the mid-high latitude lands, and even in the mid-high latitude oceans (Davis, 1976; Hu et al., 2011; 2017), which are dominated by atmospheric internal variability and minor constrained by external and/or remote forcings, such as SST (Kosaka et al., 2012; He et al., 2016). In fact, model defaults and errors in ICs (or reanalyses) may also affect the prediction skill at some extent (Kumar and Hu, 2012; Zhu et al., 2013; Liang et al., 2018).

5. Summary and discussions

This study has examined the seasonal predictability of the PEASCPs such as the WPSH, SAH, PSAC and EASM by using 26-year (1991-2016) hindcasts of the three operational climate prediction models, viz., BCC_CSM1.1(m), ECMWF System 4

and NCEP CFSv2. In addition, we also have analyzed the connection of model prediction skills with ENSO influence. Our findings can be summarized as follows:

Prediction skills are sensitive to the initial time of models, and the ensemble mean can provide relatively higher and more stable skills. The indices representing intensity and area have high predictability in models, but the predictability of position indices is relatively low. Specifically, skills of the WPSH intensity, area, SAH center intensity, PSAC and EASM are higher, while the WPSH western boundary and SAH center latitude are lower, and skills of the WPSH ridge line and SAH center longitude are the lowest. ENSO signal is the dominant source of predictability for these PEASCPs. Prediction skills are connected with ENSO. If strong ENSO events occur in observation during former winter and the models can capture the high lag-correlation between PEASCP and ENSO, the model predictions are quite reliable.

In general, models have reliable prediction skills for the PEASCPs, but there are still some problems to be solved. For example, capacities of models to predict the position variations of WPSH ridge line and SAH center longitude are still poor that is more crucial than the intensity and area in affecting the rain belt location and EASM onset (Chang et al., 1999, Liu et al., 2013, Wei et al., 2015).

In addition, on the basis of existing model prediction, statistical-dynamical method, such as analogue-based correction (Ren et al., 2014; Liu and Ren, 2015, 2017)

Author Manuscript

can be used for improving the prediction results and enhancing the prediction skills. Yang et al. (2016) also pointed out that MME can significantly improve the prediction ability of models. Therefore, statistical-dynamical method on the base of MME may be an important direction of future seasonal prediction operation.

Acknowledgments.

This work was jointly supported by the National Key Research and Development Program on monitoring, Early Warning and Prevention of Major Natural Disaster (Grant No. 2018YFC1506004, 2017YFC1502302), and the Foundation for Innovative Research Groups of the National Natural Science Foundation of China (Grant No. 41421004).

References

- Chang, C.P., Zhang, Y.S., and Li, T. (1999) Interannual and interdecadal variations of the East Asian summer monsoon and tropical Pacific SSTs. Part I: roles of the subtropical ridge. *Journal of Climate*, 13, 4310–4325.
- Cheng, Y.B., Ren, H.L., and Tan, G.R. (2016) Empirical orthogonal function analogue correction of extra-seasonal dynamical prediction of East Asian summer monsoon. *Journal of Applied Meteorological Science (in Chinese)*, 3, 285–292.
- Chou, C. (2004) Establishment of the Low-Level Wind Anomalies over the Western North Pacific during ENSO Development. *Journal of Climate*, 17, 2195–2212.
- Davis, R.E. (1976) Predictability of sea surface temperature and sea level pressure anomalies over the North Pacific Ocean. *Journal of Physical Oceanography*, 6, 249–266.
- Ding, Q.H., and Wang, B. (2005) Circumglobal teleconnection in the Northern Hemisphere summer. *Journal of Climate*, 18, 3483–3505.
- Ding, Y.H., and Chan, J.C.L. (2005) The East Asian summer monsoon: An overview. *Meteorology and Atmospheric Physics*, 89, 117–142.
- Guo, Q.Y. (1983) The summer monsoon intensity index in East Asia and its variation. *Acta Geographica Sinica (in Chinese)*, 3, 207–217.
- Han, R., Wang, H., Hu, Z.Z., Kumar, A., Li, W., Long, L., Schemm, J.K., Peng, P., Wang, W., Si, D., Jia, X., Zhao, M., Vecchi, G.A., Larow, T.E., Lim, Y.K., Schubert, S.D., Camargo, S.J., Henderson, N., Jonas, J. A., and Walsh, K.J.E. (2016) An assessment of multi-model simulations for the variability of western North Pacific tropical cyclones and its association with ENSO. *Journal of Climate*, 29, 6401–6423.
- Hu, Z.Z., Kumar, A., Huang, B., Xue, Y., Wang, W., and Jha, B. (2011) Persistent

atmospheric and oceanic anomalies in the North Atlantic from summer 2009 to summer 2010. *Journal of Climate*, 24, 5812–5830.

Hu, Z.Z., Kumar, A., Jha, B., Zhu, J., and Huang, B. (2017) Persistence and predictions of the remarkable warm anomaly in the northeastern Pacific Ocean during 2014–2016. *Journal of Climate*, 30, 689–702.

Hu, Z.Z., Kumar, A., Zhu, J., Peng, P., and Huang, B. (2019) On the challenge for ENSO cycle prediction: An example from NCEP Climate Forecast System version 2. *Journal of Climate*, 32, 183–194.

Huang, G. (2004) An index measuring the interannual variation of the East Asian summer monsoon—The EAP index. *Advances in Atmospheric Sciences*, 21, 41–52.

Kanamitsu, M., Ebisuzaki, W., Woollen, J., et al. (2002) NCEP-DOE AMIP-II reanalysis (R-2). *Bulletin of the American Meteorological Society*, 83, 1631–1643.

Kharin, V.V., and Zwiers, F.W. (2002) Climate predictions with multimodel ensembles. *Journal of Climate*, 15, 793–799.

Kirtman, B.P., Min, D., Infanti, J.M., et al. (2014) The North American Multimodel Ensemble: Phase-1 Seasonal-to-Interannual Prediction; Phase-2 toward Developing Intraseasonal Prediction. *Bulletin of the American Meteorological Society*, 95, 585–601.

Kosaka, Y., Chowdary, J.S., Xie, S.P., Min, Y.M., and Lee, J.Y. (2012) Limitations of seasonal predictability for summer climate over East Asia and the Northwestern Pacific. *Journal of Climate*, 25, 7574–7589.

Krishnamurti, T.N., Kishtawal, C.M., LaRow, T.E., et al. (1999) Improved weather and seasonal climate forecasts from a multi-model superensemble. *Science*, 286, 1548–1550.

- Kumar, A., and Hoerling, M. P. (2000) Analysis of a conceptual model of seasonal climate variability and implications for seasonal prediction. *Bulletin of the American Meteorological Society*, 81, 255–264.
- Kumar, A., and Hu, Z.Z. (2012) Uncertainty in the ocean-atmosphere feedbacks associated with ENSO in the reanalysis products. *Climate Dynamics*, 39, 575–588.
- Kumar, K.K., Hoerling, M., and Rajagopalan, B. (2005) Advancing Indian monsoon rainfall predictions. *Geophysical Research Letters*, 32, L08704.
- Kug, J.S., Kang, I.S., and Choi, D.H. (2008) Seasonal climate predictability with tier-one and tier-two prediction systems. *Climate Dynamics*, 31, 403–416.
- Lau, K.M. (2000) Dynamical and boundary forcing characteristics of regional components of the Asian summer monsoon. *Journal of Climate*, 13, 2461–2482.
- Li, W.J., Zhang, P.Q. Li, Q.Q. and et al. (2005) Research and operational application of dynamical climate model prediction system. *Journal of Applied Meteorological Science (in Chinese)*, 16, 1–11.
- Liang, P., Hu, Z.Z., Liu, Y., Yuan, X., Li, X., and Jiang, X. (2018) Challenges in predicting and simulating summer rainfall in the eastern China. *Climate Dynamics*, 52, 2217–2233. doi: 10.1007/s00382-018-4256-6.
- Liu, B.Q., Wu, G.X., Mao, J.Y., and He, J.H. (2013) Genesis of the South Asian high and its impact on the Asian summer monsoon onset. *Journal of Climate*, 26, 2976–2991.
- Liu, X.W., Wu, T.W., Yang, S., et al. (2015) Performance of the seasonal forecasting of the Asian summer monsoon by BCC_CSM1.1(m). *Advances in Atmospheric Sciences*, 32, 1156–1172.
- Liu, Y., and Ren, H.L. (2015) A hybrid statistical downscaling model for prediction

of winter precipitation in China. *International Journal of Climatology*, 35, 1309–1321.

Liu, Y., and Ren, H.L. (2017) Improving ENSO prediction in CFSv2 with an analogue-based correction method. *International Journal of Climatology*, 37, 5035–5046.

Liu, Y.Y., Li, W.J., Ai, W.X., and Li, Q.Q. (2012) Reconstruction and application of the monthly Western Pacific Subtropical high indices. *Journal of Applied Meteorological Science (in Chinese)*, 23, 414–423.

Lu, E., and Chan, J.C.L. (1999) A unified monsoon index for south China. *Journal of Climate*, 12, 2375–2385.

Lu, R.Y. (2002) Indices of the summertime western North Pacific subtropical high. *Advances in Atmospheric Sciences*, 19, 1004–1028.

Ma, J.H., and Wang, H.J. (2014) Design and testing of a global climate prediction system based on a coupled climate model. *Science China Earth Sciences*, 57, 2417–2427.

Min, Y.M., Kryjov, V.N., and Park, C.K. (2009) A probabilistic multimodel ensemble approach to seasonal prediction. *Weather & Forecasting*, 24, 812–828.

Molteni, F., Stockdale, T., Balmaseda, M.A., and et al. (2011) The new ECMWF seasonal forecast system (System 4). *ECMWF Technical Memorandum 656*.

National Research Council, 2010: Assessment of Intraseasonal to Interannual Climate Prediction and Predictability, 192 PP., ISBN-10: 0-309-15183-X, the National Academies Press, Washington, DC, USA.

Palmer, T.N., Alessandri, A., Andersen, U., et al. (2004) Development of a European Multimodel Ensemble System for Seasonal to Interannual Prediction (DEMETER). *Bulletin of the American Meteorological Society*, 85, 853–872. <https://doi.org/10.1175/BAMS-85-6-853>.

- Qian, Y.F., Zhang, Q., and Zhang, X.H. (2002) The South Asia high and its effects on China's mid-summer climate abnormality. *Journal of Nanjing University (Natural Sciences) (in Chinese)*, 38, 295–307.
- Ren, H.L., Zhang, P.Q., Li, W.J., et al. (2014) The dynamical-analogue ensemble method for improving operational monthly forecasting. *Acta Meteorologica Sinica (in Chinese)*, 72, 723–730.
- Ren, H.L., Jin, F.F., Song, L., et al. (2017) Prediction of primary climate variability modes in Beijing Climate Center. *Journal of Meteorological Research*, 31, 204–223.
- Saha, S., Moorthi, S., Wu, X.R., et al. (2014) The NCEP climate forecast system version 2. *Journal of Climate*, 27, 2185–2208.
- Shi, N., Zhu, Q.G., and Wu, B.G. (1996) The East Asian Summer monsoon in relation to summer large scale weather-climate anomaly in China for last 40 years. *Chinese Journal of Atmospheric Sciences (in Chinese)*, 20, 575–583.
- Shukla, J. (1998) Predictability in the midst of chaos: A scientific basis for climate forecasting. *Science*, 282, 728–731.
- Sun, X.R., Chen, L.X., and He, J.H. (2002) Index of land-sea thermal difference and its relation to interannual variation of summer circulation and rainfall over East Asia. *Acta Meteorologica Sinica (in Chinese)*, 60, 164–172.
- Wang, B., Wu, R.G., and Fu, X.H. (2000) Pacific-East Asian teleconnection: how does ENSO affect East Asian climate? *Journal of Climate*, 13, 1517–1536.
- Wang, B., and Zhang, Q. (2002) Pacific-East Asian Teleconnection. Part II: How the Philippine Sea Anomalous Anticyclone is Established during El Niño Development. *Journal of Climate*, 15, 3252–3265.
- Wang, B., Kang, I.S., and Lee, J.Y. (2004) Ensemble simulations of Asian–Australian monsoon variability by 11 AGCMs. *J. Climate*, 17, 803–818.

- Wang, B., Ding, Q.H., Fu, X.H., et al. (2005) Fundamental challenge in simulation and prediction of summer monsoon rainfall. *Geophysical Research Letters*, 32, L15711.
- Wang, B., Lee, J.Y., Kang, I.S., et al. (2009) Advance and prospectus of seasonal prediction: assessment of the APCC/CliPAS 14-model ensemble retrospective seasonal prediction (1980–2004). *Climate Dynamics*, 33, 93–117.
- Wang, B., and Fan, Z. (1999) Choice of South Asian summer monsoon indices. *Bulletin of the American Meteorological Society*, 80, 629–638.
- Wang, B., Xiang, B.Q., and Lee, J.Y. (2013) Subtropical high predictability establishes a promising way for monsoon and tropical storm predictions. *Proceedings of the National Academy of Sciences*, 110, 2718–2722.
- Wang, H.J. (2001) The weakening of the Asian monsoon circulation after the end of 1970's. *Advances in Atmospheric Sciences*, 18, 376–386.
- Wang, H.J. (2002) Instability of the East Asian summer monsoon—ENSO relations. *Advances in Atmospheric Sciences*, 19, 1–11.
- Wang, H.J., Fan, K., Sun, J.Q., et al. (2015) A review of seasonal climate prediction research in China. *Advances in Atmospheric Sciences*, 32, 149–168.
- Watanabe, M., Jin, F.F. (2002) Role of Indian Ocean warming in the development of Philippine Sea anticyclone during ENSO. *Geophysical Research Letters*, 29, 1478.
- Wei, W., Zhang, R.H., Wen, M., and Nam, J.C. (2015) Interannual Variation of the South Asian High and Its Relation with Indian and East Asian Summer Monsoon Rainfall. *Journal of Climate*, 28, 2623–2634.
- Weisheimer, A., Doblas-Reyes, F.J., Palmer, T.N., and et al. (2009) ENSEMBLES: A new multi-model ensemble for seasonal-to-annual predictions-Skill and progress beyond DEMETER in forecasting tropical Pacific SSTs. *Geophys. Res.*

Lett., 36, L21711.

- Wu, A., and Ni, Y. (1997) The Influence of Tibetan Plateau on the interannual variability of Asian monsoon. *Advances in Atmospheric Sciences*, 14, 491–504.
- Wu, B., Zhou, T.J., and Li, T. (2009) Seasonally evolving dominant interannual variability modes of East Asian climate. *Journal of Climate*, 22, 2992–3005.
- Wu, R.G., Hu, Z.Z., and Kirtman, B.P. (2003) Evolution of ENSO-related rainfall anomalies in East Asia. *Journal of Climate*, 16, 3742–3758.
- Wu, R.G., and Kirtman, B.P. (2005) Roles of Indian and Pacific Ocean air–sea coupling in tropical atmospheric variability. *Climate Dyn.*, 25, 155–170.
- Wu, T.W., Song, L.C., Li, W.P., et al. (2014) An overview of BCC climate system model development and application for climate change studies. *Journal of Meteorological Research*, 28, 34–56.
- Xie, S.P., Hu, K., Hafner, J., et al. (2009) Indian Ocean capacitor effect on Indo-western Pacific climate during the summer following El Nino. *Journal of Climate*, 22, 730–747.
- Xue, F., Zeng, Q.C., Huang, R.H., et al. (2015) Recent advances in monsoon studies in China. *Advances in Atmospheric Sciences*, 32, 206–229.
- Yang, D.J., Yang, X.Q., Ren, X.J., et al. (2016) Probabilistic versus deterministic skill in predicting the western North Pacific-East Asian summer monsoon variability with multimodel ensembles. *Journal of Geophysical Research: Atmospheres*, 121, 1079–1103.
- Yang, R.W., Xie, Z.A., and Cao, J. (2017) A Dynamic Index for the Westward Ridge Point Variability of the Western Pacific Subtropical High during Summer. *Journal of Climate*, 30, 3325–3341.
- Zeng, Q.C., Yuan, C.G., Wang, W.Q., and Zhang, R.H. (1990) Experiments in numerical extraseasonal prediction of climate anomalies. *Chinese J. Atmos. Sci.*

(in Chinese), 14, 10–25.

- Zeng, Q.C., Yuan, C.G., Li, X., and et al. (1997) Seasonal and Extraseasonal predictions of summer monsoon precipitation by GCMs. *Adv. Atmos. Sci.*, 14, 163–176.
- Zhang, Q., Qian, Y.F., and Zhang, X.H. (2000) Interannual and interdecadal variations of the South Asia high. *Chinese Journal of Atmospheric Sciences (in Chinese)*, 24, 67–78.
- Zhang, Q., and Wu, G.X. (2001) The large area flood and drought over Yangtze river valley and its relation to the South Asia high. *Acta Meteorologica Sinica (in Chinese)*, 59, 569–577.
- Zhang, Q., Wu, G.X., and Qian, Y.F. (2002) The bimodality of the 100 hPa South Asia high and its relationship to the climate anomaly over East Asia in summer. *Journal of the Meteorological Society of Japan*, 80, 733–744.
- Zhang, Q.Y., Tao, S.Y., and Chen, L.T. (2003) The inter-annual variability of East Asian summer monsoon indices and its association with the pattern of general circulation over East Asia. *Acta Meteorologica Sinica (in Chinese)*, 61, 559–568.
- Zhao, P., and Zhou, Z.J. (2009) An East Asian subtropical summer monsoon index and its relationship to summer rainfall in China. *Acta Meteorologica Sinica*, 23, 18–28.
- Zhou, B., He, J.H., Wu, G.X., and Han, G.R. (2003) Characteristics of East Asian subtropical monsoon index and its definition. *Chinese Journal of Atmospheric Sciences (in Chinese)*, 27, 123–135.
- Zhou, T.J., Wu, B., and Wang, B. (2009) How well do atmospheric general circulation models capture the leading modes of the interannual variability of the Asian–Australian monsoon? *J. Climate*, 22, 1159–1173.
- Zhou, T.J., and Zou, L.W. (2010) Understanding the predictability of East Asian

summer monsoon from the reproduction of land–sea thermal contrast change in AMIP-Type simulation. *Journal of Climate*, 23, 6009–6026.

Zhu, J.S., Huang, B.H., Hu, Z.Z., Kinter, J.L., and Marx, L. (2013) Predicting U.S. summer precipitation using NCEP Climate Forecast System version 2 initialized by multiple ocean analyses. *Climate Dynamics*, 41, 1941–1954.

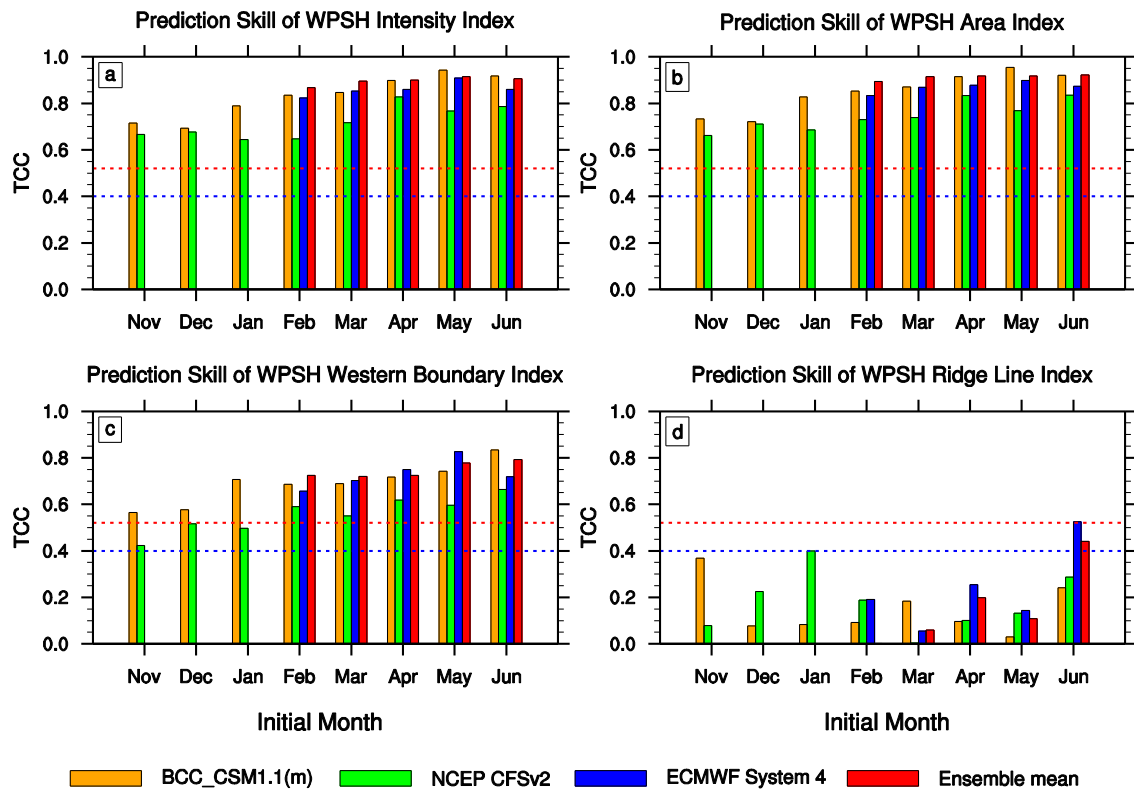


FIGURE 1 TCC skills of JJA mean WPSH intensity (a), area (b), western boundary (c), and ridge line (d) indices predicted by BCC_CSM1.1(m) (orange), NCEP CFSv2 (green), ECMWF System 4 (blue) models and the ensemble mean (red) of these three models as a function of initial calendar months. The dashed blue (red) line denotes the statistical significance at 95% (99%) confidence level based on the Student's t-test.

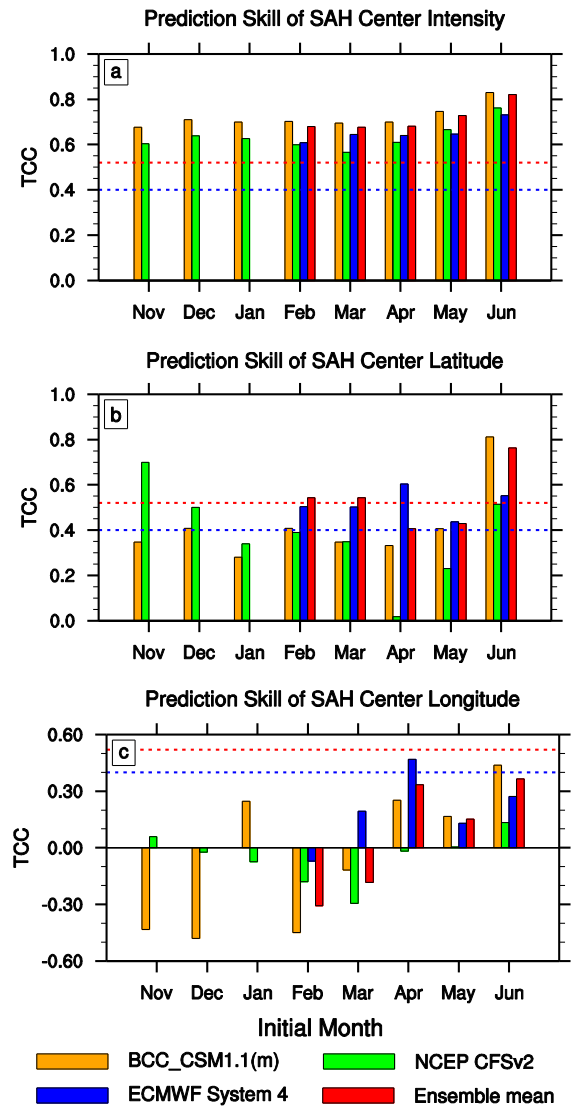


FIGURE 2 As in Figure 1, but for the SAH center intensity (a), center latitude (b), and center longitude (c) indices.

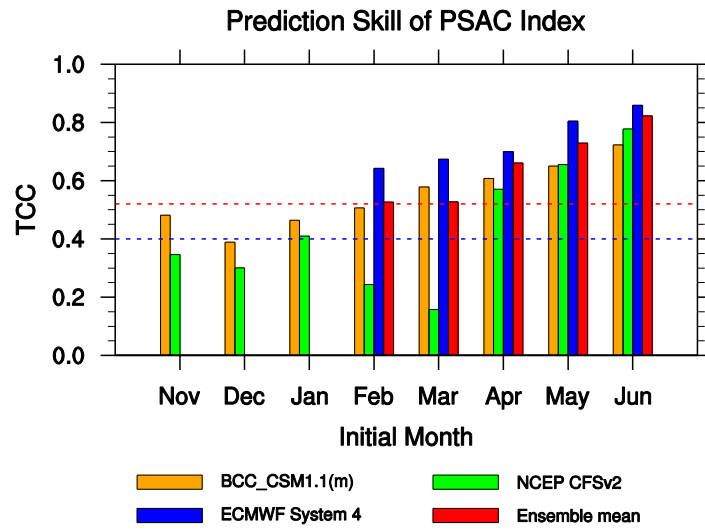


FIGURE 3 As in Figure 1, but for the PSAC index.

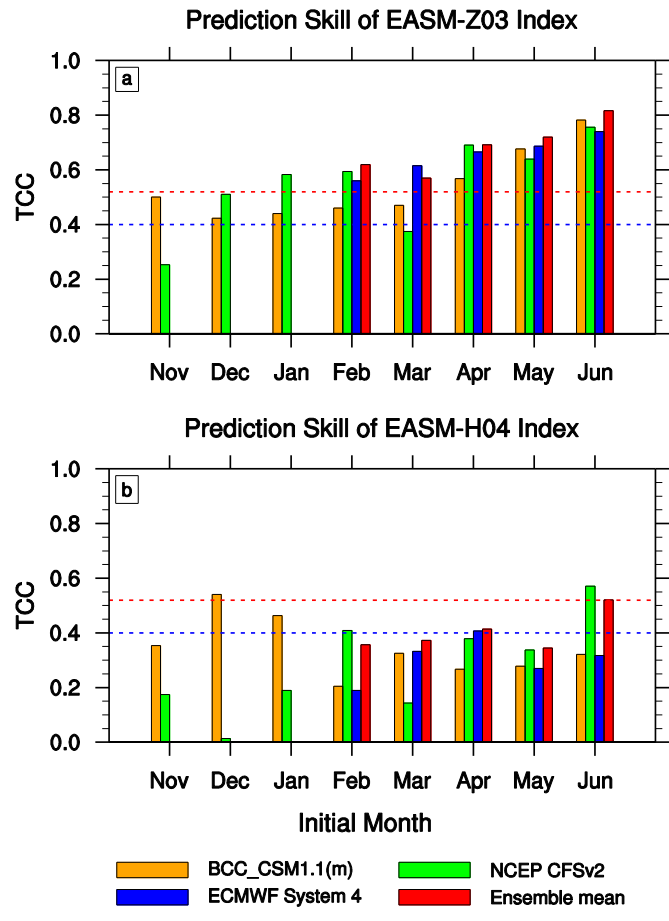


FIGURE 4 As in Figure 1, but for the EASM-Z03 (a), and EASM-H04 (b) indices.

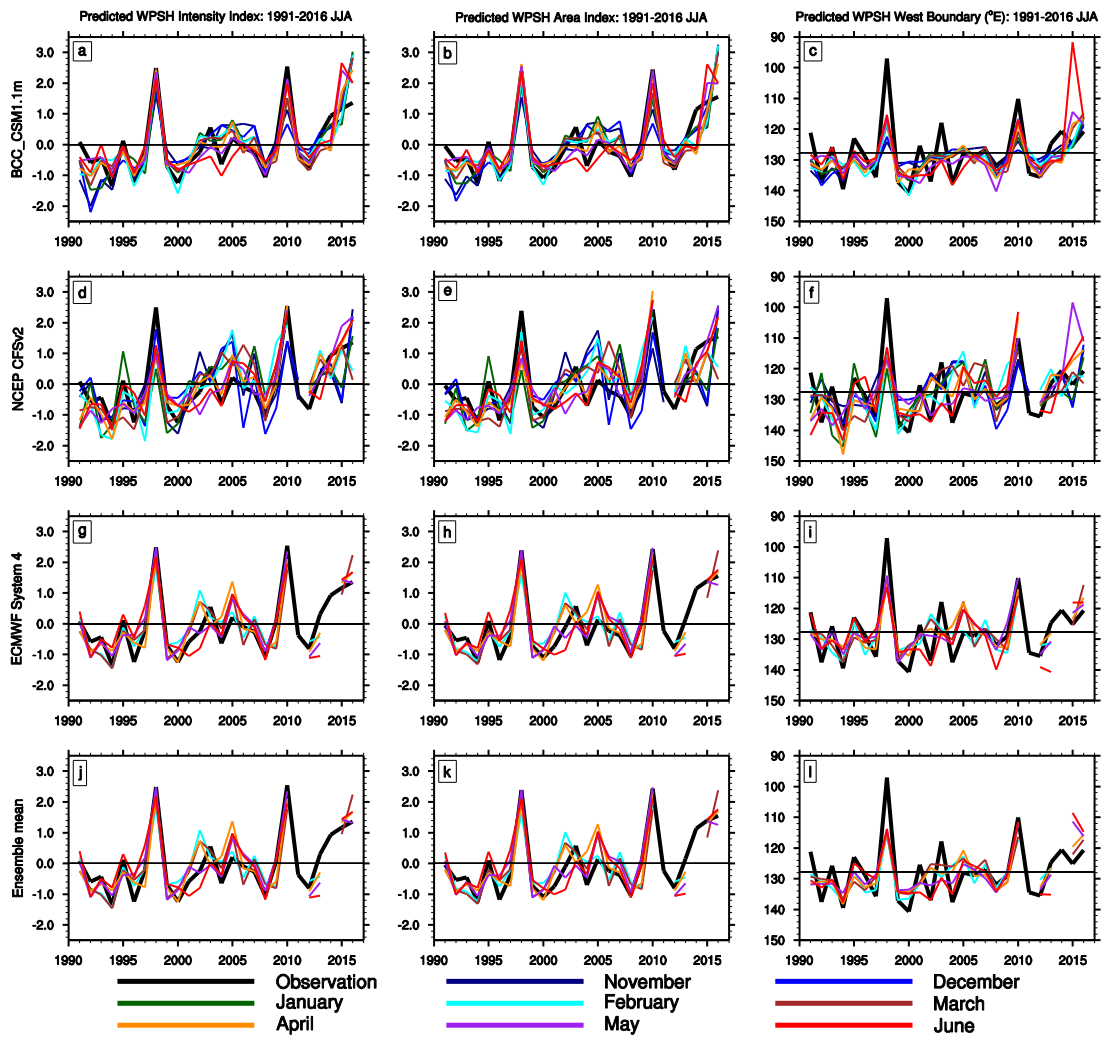


FIGURE 5 Time series of the JJA mean WPSH intensity (a, d, g, j), area (b, e, h, k), and western boundary (c, f, i, l) indices from the observation (thick black line) and model predictions (thin colored lines, for different initial months) for the period from 1991 to 2016. (a, b, c) BCC_CSM1.1(m), (d, e, f) NCEP CFSv2, (g, h, i) ECMWF System 4, and (j, k, l) ensemble mean.

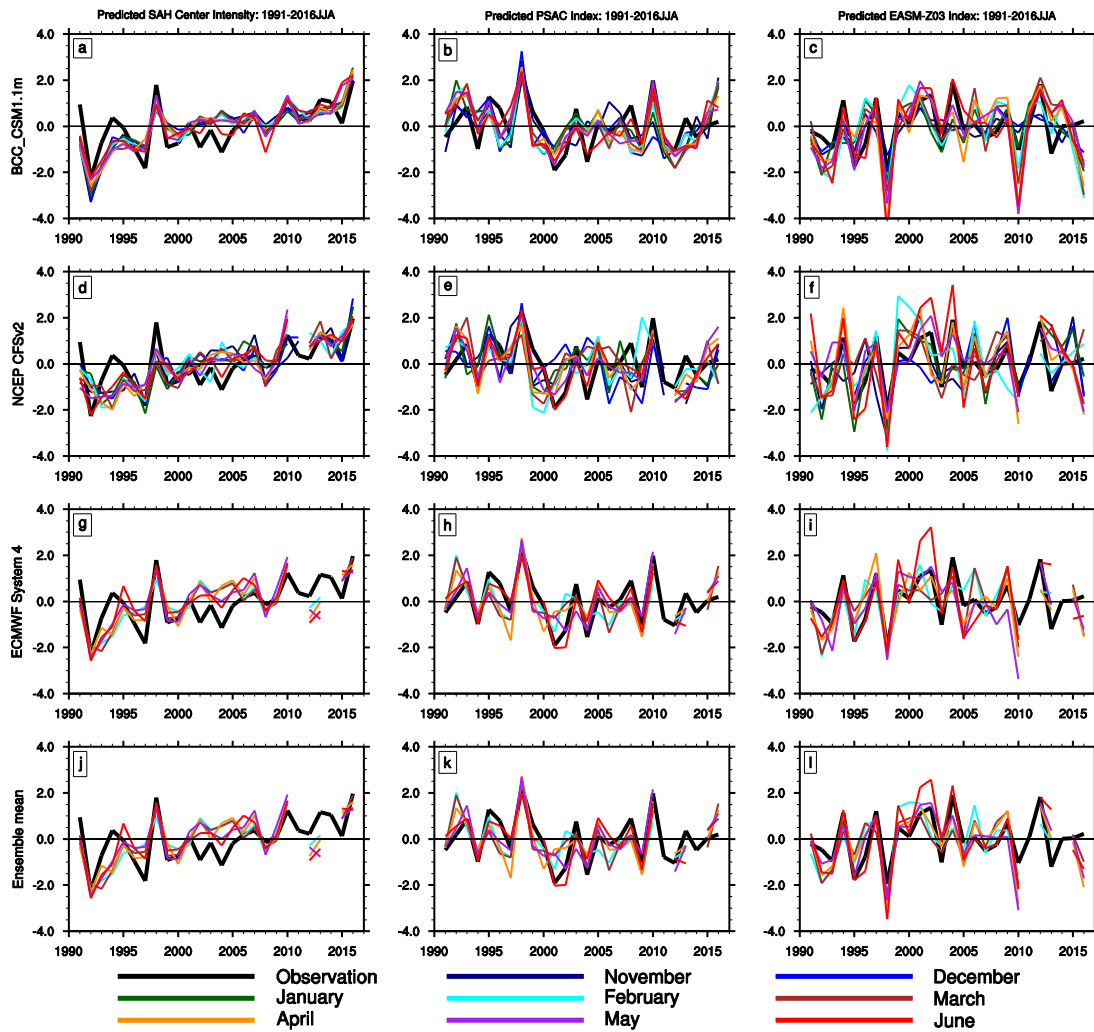


FIGURE 6 Time series of the JJA SAH center intensity (a, d, g, j), PSAC (b, e, h, k), and EASM-Z03 (c, f, i, l) indices from the observation (thick black line) and model predictions (thin colored lines, for different initial months) for the period from 1991 to 2016. (a, b, c) BCC_CSM1.1(m), (d, e, f) NCEP CFSv2, (g, h, i) ECMWF System 4, and (j, k, l) ensemble mean.

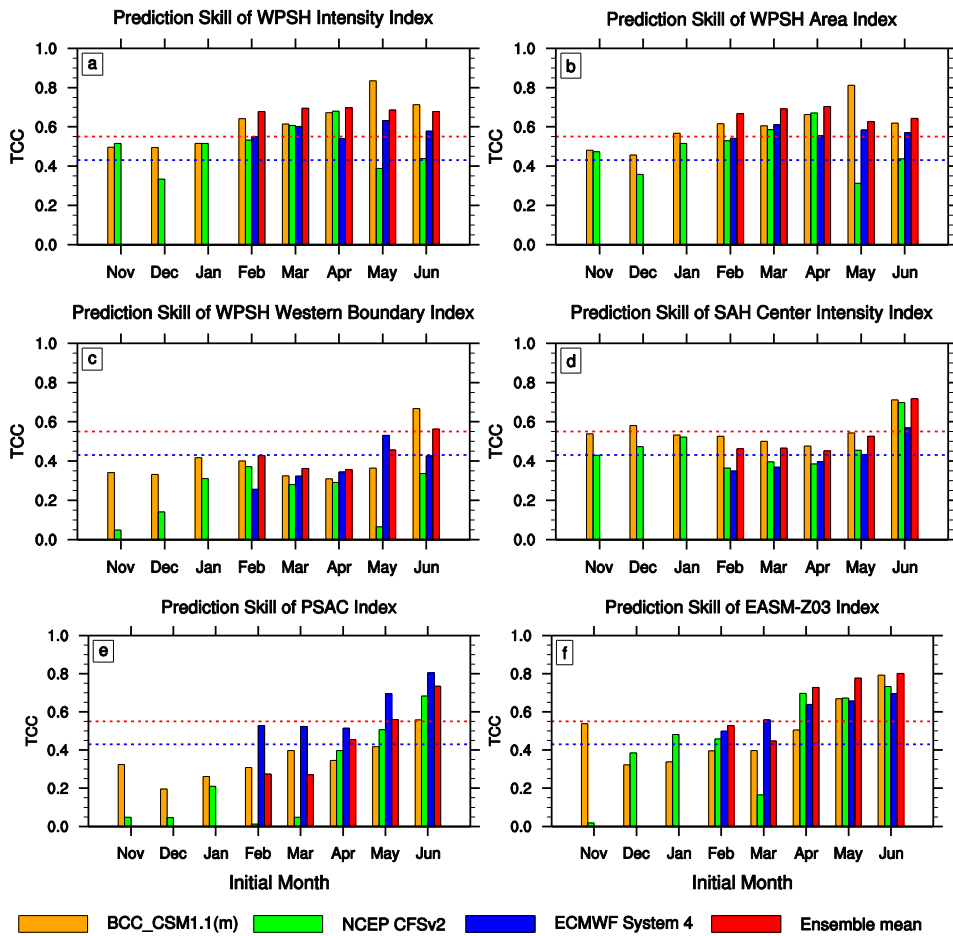


FIGURE 7 TCC skills of JJA mean WPSH intensity (a), WPSH area (b), WPSH western boundary (c), SAH center intensity (d), PSAC (e), and EASM-Z03 (f) indices predicted by BCC_CSM1.1(m) (orange), NCEP CFSv2 (green), ECMWF System 4 (blue) models and the ensemble mean (red) of these three models as a function of initial calendar months, eliminating the years of 1998, 2010 and 2016. The dashed blue (red) line denotes the statistical significance at 95% (99%) confidence level based on the Student's t-test.

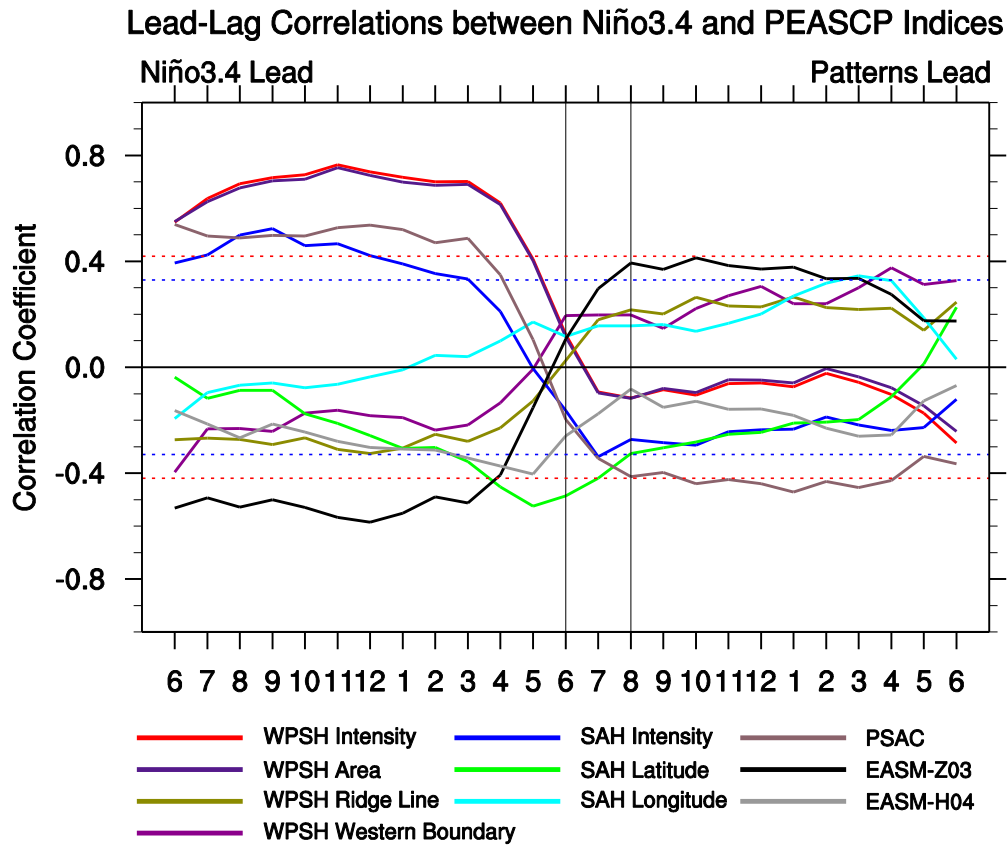


FIGURE 8 Lead-lag correlations between observed JJA mean circulation pattern indices and observed monthly Niño3.4 index. Colors are for different circulation pattern indices. Dashed blue (red) line denotes the statistical significance at 95% (99%) confidence level based on the Student's t-test.

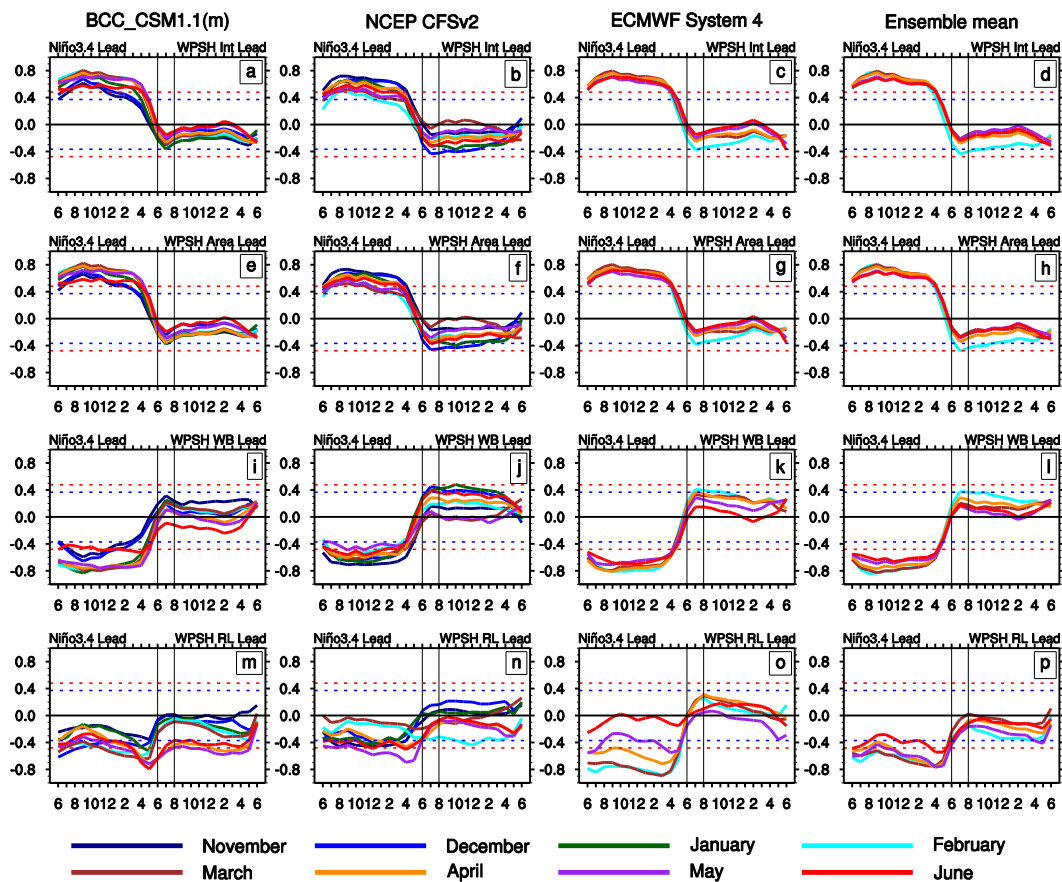


FIGURE 9 Lead-lag correlations between predicted JJA mean WPSH intensity (a, b, c, d), area (e, f, g, h), western boundary (i, j, k, l) and ridge line (m, n, o, p) indices and observed monthly Niño3.4 index, where (a, e, i, m), (b, f, j, n), (c, g, k, o), (d, h, l, p) are for BCC_CSM1.1(m), NCEP CFSv2, ECMWF System 4 models and ensemble mean, respectively. Colors are for different initial months. Dashed blue (red) line denotes the statistical significance at 95% (99%) confidence level based on the Student's t-test.

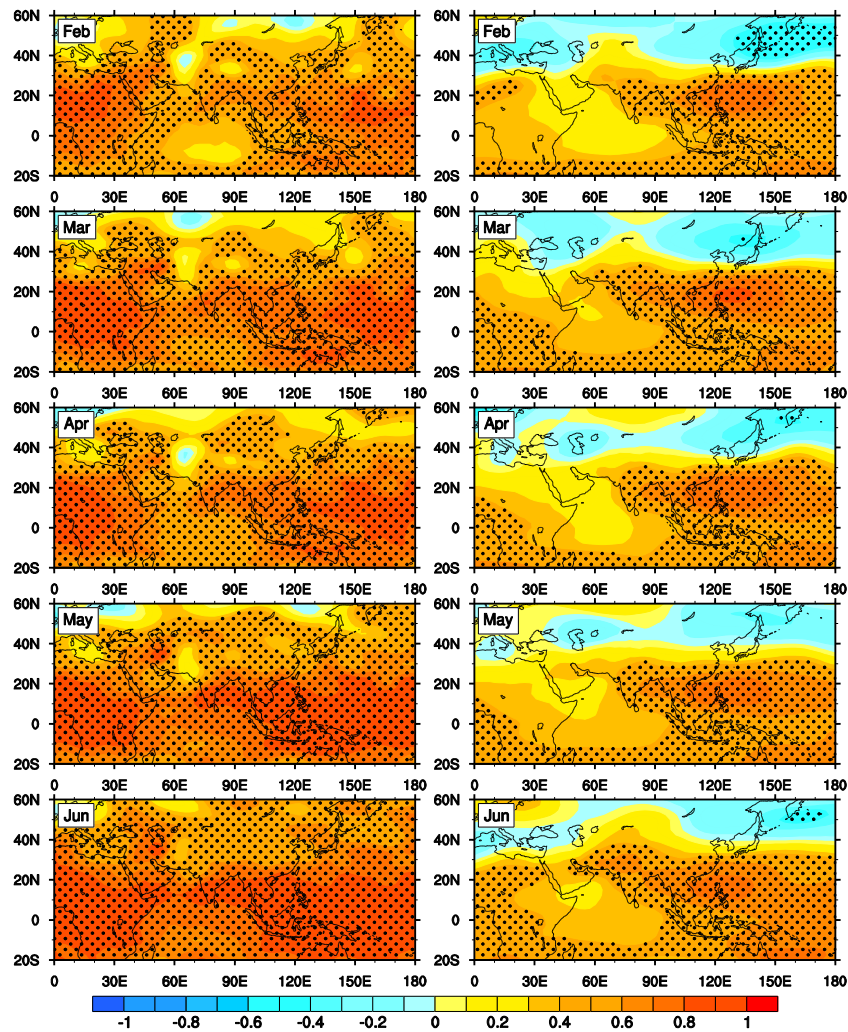


FIGURE 10 (Left panel) Spatial pattern of the TCC skills of JJA H500 for ensemble mean for ICs in Feb-Jun. (Right panel) Lag correlation coefficients of observed DJF Niño3.4 index on JJA H500 for ensemble mean for ICs in Feb-Jun. Black dots denote the statistical significance at 95% confidence level based on the Student's t-test.

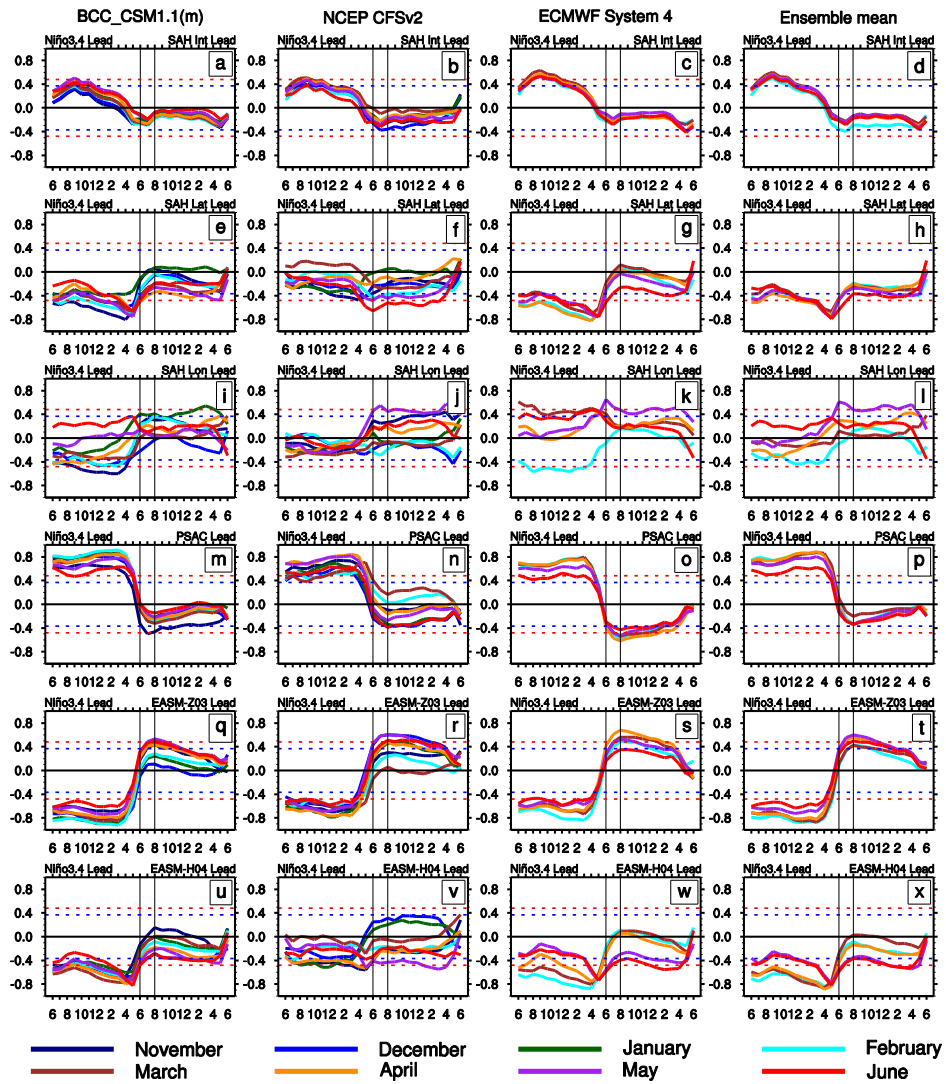
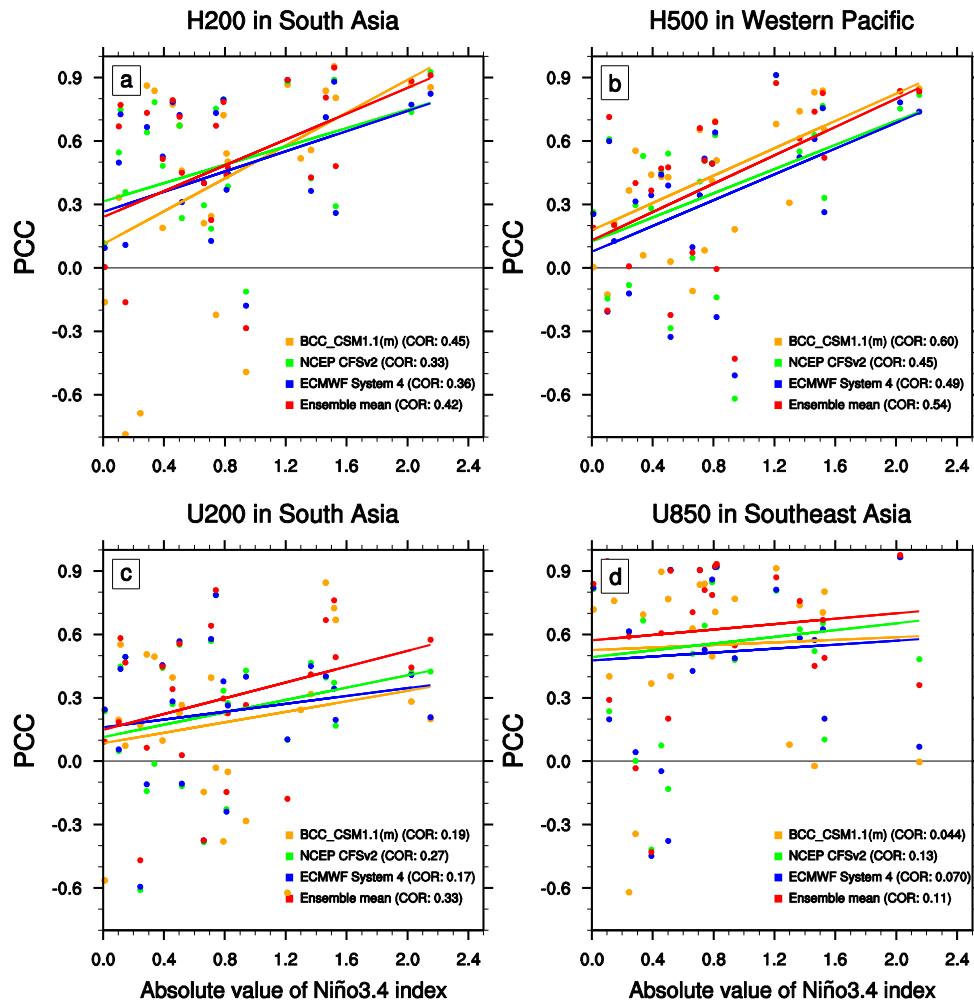


FIGURE 11 Lead-lag correlations between predicted JJA mean SAH center intensity (a, b, c, d), latitude (e, f, g, h), longitude (i, j, k, l), PSAC (m, n, o, p), EASM-Z03 (q, r, s, t) and EASM-H04 (u, v, w, x) indices and observed monthly Niño3.4 index, where (a, e, i, m, q, u), (b, f, j, n, r, v), (c, g, k, o, s, w), (d, h, l, p, t, x) are for BCC_CSM1.1(m), NCEP CFSv2, ECMWF System 4 models and ensemble mean, respectively. Colors are for different initial months. Dashed blue (red) line denotes the statistical significance at 95% (99%) confidence level based on the Student's t-test.



1

2 **FIGURE 12** Scatter plots and linear regression lines of PCC skills for
 3 BCC_CSM1.1(m) (orange), NCEP CFSv2 (green), ECMWF System 4 (blue) models
 4 and the ensemble mean (red) initiated in May against the absolute value of former
 5 winter-(December, January and February)-mean Niño3.4 index: (a) geopotential
 6 height at 200 hPa over the South Asia region [10°–50°N, 30°–120°E], (b)
 7 geopotential height at 500 hPa over the Western Pacific region [10°–40°N, 90°–
 8 180°E], (c) u-wind at 200 hPa over the South Asia region [10°–50°N, 30°–120°E],
 9 and (d) u-wind at 850 hPa over the Southeast Asia region [10°–20°N, 90°–120°E].

Table 1 Information of models adopted in this study

model	prediction time	initialized date	time period
BCC_CSM1.1(m)	12 months	15th of each month	1991 to present
NCEP CFSv2	9 months	18th of each month	1982 to present
ECMWF System 4	7 months	10th of each month	1981 to present

Table 2 Definitions of PEASCP indices applied in this study

PEASCP	index	definition	illustration
WPSH	area	$WPSH_{\text{area}} = \sum_i A(i) \text{ (gh}(i) \geq 588 \text{dagpm)}$	A(i) and gh(i) denote the area and geopotential height of grid <i>i</i> at 500 hPa isobaric level, respectively. Each index is calculated in the region of 10°–90°N, 110°E–180° (Liu et al., 2012)
	intensity	$WPSH_{\text{int}} = \sum_i A(i) * (\text{gh}(i) - 587 \text{dagpm}) \text{ (gh}(i) \geq 588 \text{dagpm)}$	
	western boundary	The longitude of the westernmost grid at 588 dagpm contour line. If the longitude locates at the west of 90°E, the western boundary index will be uniformly recorded as 90°E.	
	ridge line	The averaged 0 line of $\partial \text{gh} / \partial y$ in the area of [10°–45°N, 110°–150°E].	
SAH	center latitude	The latitude of maximum geopotential height position from the contour line where the u-wind equals 0 around [10°–55°N, 35°–115°E] at 200 hPa isobaric level.	Here we only consider the maximum value center of the SAH if there exists bimodality. (Zhang et al., 2000, 2002; Qian et al., 2002)
	center longitude	The longitude of maximum geopotential height position from the contour line where the u-wind equals 0 around [10°–55°N, 35°–115°E] at 200 hPa isobaric level.	
	center intensity	The geopotential height value (minus 1600 dagpm) of the center.	
PSAC	intensity	The area average of SLP anomalies over the Philippine Sea region [10°–20°N, 120°–150°E].	Wang et al. (2000, 2002)
EASM	intensity	The difference of 850 hPa zonal wind anomalies between tropical monsoon trough area in East Asia [10°–20°N, 100°–150°E] and subtropical East Asia area [25°–35°N, 100°–150°E] (denoted as EASM–Z03).	Zhang et al. (2003)
	intensity	Based on the EAP teleconnection pattern (denoted as EASM–H04): $EASM\text{-}H04 = -0.25Z'(60^\circ\text{N}, 125^\circ\text{E}) + 0.5Z'(40^\circ\text{N}, 125^\circ\text{E}) - 0.25Z'(20^\circ\text{N}, 125^\circ\text{E})$.	$Z' = Z * \sin 45 / \sin \varphi$ is the standardized seasonal mean 500 hPa geopotential height anomaly at a grid point with the latitude φ . (Huang, 2004)